PHYSICAL REVIEW B **83**, 201104(R) (2011)

Evolution of surface states in $Bi_{1-x}Sb_x$ alloys across the topological phase transition

H. Guo,[1,2] K. Sugawara,[3] A. Takayama,[1] S. Souma,[3] T. Sato,[1] N. Satoh,[4] A. Ohnishi,[5] M. Kitaura,[5] M. Sasaki,[5] Q.-K. Xue,[2,3] and T. Takahashi[1,3]

[1]*Department of Physics, Tohoku University, Sendai 980-8578, Japan*

[2]*Department of Physics, Tsinghua University, Beijing 100084, China*

[3]*WPI Research Center, Advanced Institute for Materials Research, Tohoku University, Sendai 980-8577, Japan*

[4]*Department of Electronics and Computer Science, Iwaki Meisei University, Iwaki, Fukushima 970-8551, Japan*

[5]*Department of Physics, Faculty of Science, Yamagata University, Yamagata 990-8560, Japan*

(Received 7 March 2011; revised manuscript received 20 April 2011; published 31 May 2011)

We performed a systematic, high-resolution, angle-resolved photoemission spectroscopy of $Bi_{1-x}Sb_x$ alloys to study the evolution of electronic states as a function of Sb concentration x. We revealed that the number of Fermi-level crossings is different between the topologically trivial ($x = 0.023$) and nontrivial ($x = 0.17$) phases: four and five times for the former and latter cases, respectively. We also found a systematic expansion of the bandwidth of spin-split surface bands at the $\bar{\Gamma}$ point upon substituting Bi with Sb, which is indicative of the monotonous reduction of the spin-orbit coupling strength.

DOI: 10.1103/PhysRevB.83.201104 PACS number(s): 73.20.−r, 79.60.−i, 71.20.−b

Topological insulators (TIs) are a new state of quantum matter where the strong spin-orbit coupling (SOC) plays an essential role in the realization of exotic quantum phenomena such as the quantum spin Hall effect. The first TI was found in a two-dimensional (2D) HgTe/CdTe quantum well with a one-dimensional (1D) edge state characterized by the quantized conductivity.[1,2] In analogy to the 2D case, it is expected that 2D surface states would appear in three-dimensional (3D) TIs. Such a surface state, as revealed by a few experimental techniques[3–17] including angle-resolved photoemission spectroscopy (ARPES), would provide a novel platform to study the peculiar topological properties like robustness against disorder[18,19] and dissipationless spin transport.[12]

It has been theoretically proposed that $Bi_{1-x}Sb_x$ would be a 3D TI.[20] As shown in Fig. 1(a), alloying Bi with Sb leads to the inversion of the valence-band parity at the L point in the bulk Brillouin zone (BZ) at $x \sim 0.023$, where the system undergoes the transition from the topologically trivial (topological invariant $Z_2 = 0$) to the nontrivial ($Z_2 = 1$) phase. It is also clear from Fig. 1(a) that the bulk insulating phase appears in the region of $0.07 < x < 0.23$.[20] ARPES and subsequent spin-resolved photoemission experiments have clarified that $Bi_{1-x}Sb_x$ at $x = 0.10$ belongs to the TI phase by elucidating the surface band structure[8] and the overall helical spin texture.[9] A recent spin-resolved ARPES experiment for $x = 0.12$–0.13 has revealed the detailed spin configuration to give conclusive evidence for the TI phase.[10]

Although previous ARPES experiments have thus established the TI character for $Bi_{1-x}Sb_x$, there are a few unresolved issues yet to be clarified. For example, the configuration proposed thus far of the surface band structure in the TI phase is markedly different between ARPES experiments and the theories, and even within the theories and experiments.[8,10,11,21,22] This point is crucial in constructing an elaborated microscopic model to describe the physical properties of the TI phase, since the band configuration information [specifically the number of band crossings (even or odd)] is indispensable for the classification of TIs.[12] Indeed, an ARPES experiment for $x = 0.10$ (Ref. 8) reported three surface bands (Σ_1, Σ_2, and Σ_1') which cross the Fermi level (E_F) at five points between the two time-reversal invariant momenta $\bar{\Gamma}$ and $\bar{M}$ [Fig. 1(c)]. However, none of the theoretical calculations could correctly reproduce the presence of the observed third band Σ_1' near the $\bar{M}$ point, and, furthermore, the band configuration for the Σ_1 and Σ_2 bands is different between the *ab initio*[21] and the tight-binding calculations[22] [Figs. 1(d) and 1(e)]. Experimentally, the number of E_F crossings along the $\bar{\Gamma}\bar{M}$ cut is different between different ARPES experiments [5 times for $x = 0.10$ (Ref. 8) and 3 times for $x = 0.12$–0.13 (Ref. 10), as shown in Figs. 1(c) and 1(f), respectively]. These controversial results clearly require a systematic ARPES measurement as a function of x.

In this Rapid Communication, we report our high-resolution ARPES results on $Bi_{1-x}Sb_x$ with a wide range of Sb concentrations ($x = 0.0$, 0.023, 0.17, and 1.0). We found that the overall Fermi surface (FS) and the band structure of the surface states are similar between the nontopological and the topological phases near the phase boundary, while the Σ_1' band appears only in the TI phase, resulting in the difference in the number of band crossings across the topological phase transition. We found a systematic variation in the band structure at the $\bar{\Gamma}$ point as a function of x, which would reflect a gradual reduction of the SOC strength.

Single crystals of $Bi_{1-x}Sb_x$ alloy were grown by the Bridgeman method. The purity of the starting material was 99.9999% for Bi and Sb. The Sb composition x was determined by energy dispersive x-ray diffraction experiments. High-resolution ARPES measurements were performed by using a VG-Scienta SES2002 and a MBS-A1 spectrometer with high-flux helium and xenon discharge lamps[23] at Tohoku University. The He Iα ($h\nu = 21.218$ eV) and one Xe I ($h\nu = 8.437$ eV) lines were used to excite the photoelectrons. Samples were cleaved *in situ* along the (111) crystal plane in an ultrahigh vacuum of 5×10^{-11} Torr. The energy and angular resolutions were set at 4–15 meV and 0.2°, respectively. All the samples were measured within 24 hours after cleaving, during which we did not observe any indications of surface degradation or contamination.

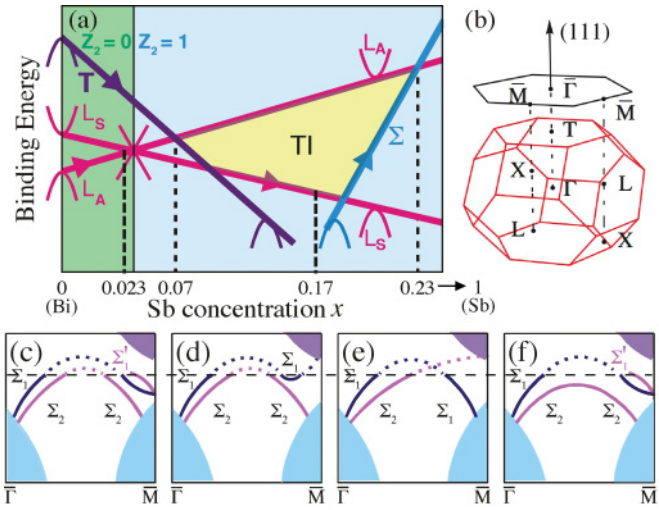

FIG. 1. (Color online) (a) Proposed phase diagram of $Bi_{1-x}Sb_x$. (Ref. 20) Green (dark gray) and light blue (light gray) regions represent topologically trivial and nontrivial phases, with $Z_2 = 0$ and 1, respectively, while the light yellow (white) region represents the TI phase. (b) 3D BZ of $Bi_{1-x}Sb_x$ with the rhombohedral structure and projected surface BZ onto the (111) plane. (c)–(f) Proposed band configurations for the TI phase by (c) ARPES measurement at $x = 1.0$ (Ref. 8), (d) *ab initio* band calculations (Ref. 21), (e) tight-binding band calculations (Ref. 22), and (f) ARPES experiment at $x = 0.12$–0.13 (Ref. 10). Light blue (light gray) and purple (dark gray) shaded regions represent the projection of valence and conduction bands, respectively.

Figures 2(a) and 2(b) display the obtained FS of $Bi_{1-x}Sb_x$ samples for trivial ($x = 0.023$) and nontrivial ($x = 0.17$) phases, respectively, measured with the He Iα line. In both samples, we find a small hexagonal FS (S_1) centered at the $\bar{\Gamma}$ point and surrounding elongated pockets (S_2), together with the ellipsoidal pocket (S_3) near the $\bar{M}$ point. Judging from the band dispersion along the $\bar{\Gamma}\bar{M}$ line [Figs. 2(c) and 2(d)], the S_1 and S_3 FSs are ascribed to the electron pockets, while the S_2 FS is ascribed to the hole pocket, which is basically consistent with the previous ARPES studies of $Bi_{1-x}Sb_x$ (Refs. 8 and 11) and pristine Bi.[24,25] All of these bands and FSs are attributed to the surface states. The broader nature of the ARPES intensity in the FS and the band-structure plot for $x = 0.17$ with respect to those for $x = 0.023$ may be due to the stronger alloying-induced disorder. To obtain further insight into the correspondence between the observed band dispersion and the previously proposed band configurations, it is particularly important to determine the band structure above E_F, because the proposed theoretical models are controversial, especially in the unoccupied states [see, e.g., Figs. 1(d) and 1(e)]. For this reason, we measured ARPES spectra at room temperature with improved statistics using the Xe I line to make use of thermally populated electrons above E_F due to the broadening of the Fermi-Dirac distribution (FD) function. The obtained ARPES intensity plot at $T = 300$ K for $x = 0.023$ is displayed in Fig. 2(e). In order to see more clearly the band dispersion above E_F, we divided the ARPES intensity with the FD function convoluted with the instrumental resolution; the result is shown in Fig. 2(f). It is evident that the Σ_2 band near the $\bar{\Gamma}$ point is smoothly connected to the dispersive feature near the $\bar{M}$ point, with the top of the dispersion ~20 meV above E_F (see dashed curve Σ_2). Moreover, the Σ_1 band is highly dispersive above E_F and disperses beyond -0.1 eV. From these results, we conclude that the Σ_1 and Σ_2 bands do not cross each other, unlike the tight-binding calculations [Fig. 1(e)].

The next important issue is the existence or absence of the third band Σ_1' near the $\bar{M}$ point. To clarify this point, we performed high-resolution measurements along the cut, as shown in Fig. 3(a). The corresponding ARPES intensity for $x = 0.17$ is displayed in Fig. 3(b). A holelike Σ_2 band with a top of 0.12 eV and an electronlike Σ_1 band near E_F are clearly identified. To examine the emergence of the Σ_1' band, we display in Fig. 3(c) the energy distribution curve (EDC) for $x = 0.17$ in the region denoted by a red line in Fig. 3(b), compared with the same plot for $x = 0.023$. The EDC for $x = 0.17$ has a peak at 35 meV, which originates in the Σ_1 band, together with a large shoulderlike feature near E_F, while such a shoulder is not seen for $x = 0.023$. In fact, when we numerically simulate the EDC using Gaussians, the EDC for $x = 0.17$ is well reproduced by two Gaussians centered at 35 and 10 meV (for the Σ_1 and Σ_1' bands, respectively), while the peak (from the Σ_1 band) for $x = 0.023$ is satisfactorily reproduced by a single Gaussian at 25 meV. This suggests that the Σ_1' band appears only in the TI phase, as schematically shown by the inset in Fig. 3(c). As a consequence, the number

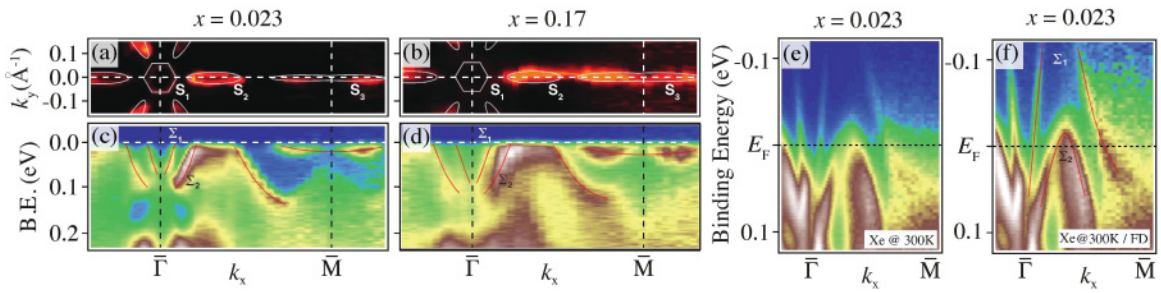

FIG. 2. (Color online) (a), (b) ARPES intensity plot at E_F of $Bi_{1-x}Sb_x$ as a function of 2D wave vector for $x = 0.023$ and 0.17, respectively, measured with the He Iα line. The intensity is integrated over ± 20 meV with respect to E_F. (c), (d) ARPES intensity plot as a function of k_x and binding energy (B. E.) along the $\bar{\Gamma}\bar{M}$ cut for $x = 0.023$ and 0.17, respectively. (e) ARPES intensity plot along the $\bar{\Gamma}\bar{M}$ cut for $x = 0.023$ measured with the Xe I line at 300 K. (f) Same as (e) but divided by the FD function at 300 K convoluted with the instrumental resolution. Red curves in (c), (d), and (f) are a guide for eyes to trace the band dispersion.

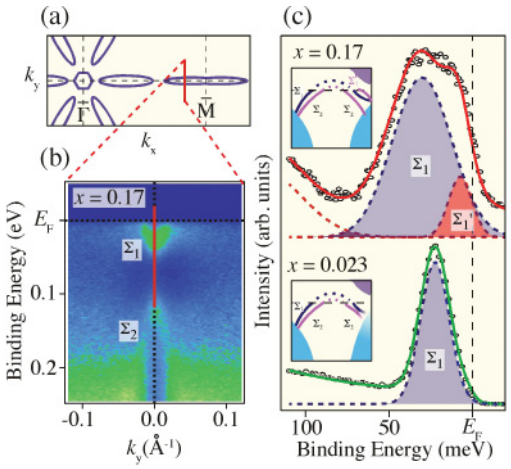

FIG. 3. (Color online) (a) Schematic FS of $Bi_{1-x}Sb_x$ with the measured cut (red line). (b) ARPES intensity at $T = 30$ K as a function of k_y and binding energy for $x = 0.17$. (c) Comparison of near-E_F EDCs between $x = 0.023$ and 0.17 measured at the cut shown by a red (gray) line in (b). Results of fitting with single or double Gaussian(s) with a moderate background are indicated by solid curves. Inset shows the schematic band configuration for each composition determined from the present ARPES experiment.

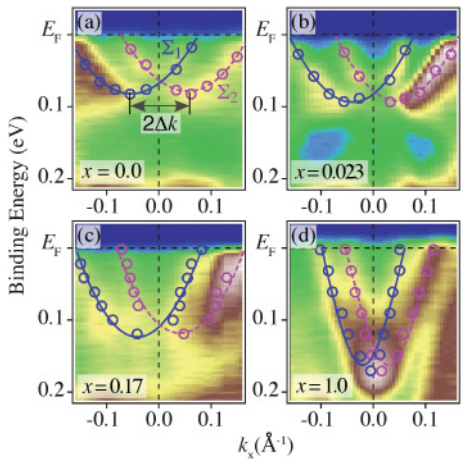

FIG. 4. (Color online) Comparison of ARPES intensity around the $\bar{\Gamma}$ point as a function of binding energy and k_x measured for samples with various x values (0.0, 0.023, 0.17, and 1.0). Blue (gray) and purple (light gray) circles represent estimated energy positions of the EDC peaks, and the solid curves represent the result of fitting by assuming a simple Rashba splitting with the dispersion relation $E(k) = a(k \pm \Delta k)^2 - E_0$, where $2\Delta k$ is the momentum separation of spin-split bands and E_0 is the bottom of the energy band. Length of $2\Delta k$ is also indicated in (a).

of band crossings along the $\bar{\Gamma}\bar{M}$ direction becomes 5 and 4 for $x = 0.17$ and 0.023, respectively, which satisfies the criteria of topologically nontrivial and trivial phases ($Z_2 = 1$ and 0).

Here we comment on the band configuration in the inset of Fig. 3(c). Because of the requirement from the time-reversal symmetry,[26] the Σ_1 and Σ_2 bands for both $x = 0.17$ and 0.023 should theoretically cross each other at the $\bar{\Gamma}$ point, and the Σ_2 band and another surface band for $x = 0.17$ should cross each other at the $\bar{M}$ point, while these features are hindered by the bulk-band projection (light blue regions). It is also noted that the Σ_1 band (and also the Σ_2 band) for $x = 0.023$ should coincide with another surface band at the $\bar{M}$ point, although such a degeneracy is not clearly resolved in the present ARPES experiment. We think that the difficulty in observing the Kramers degeneracy at the $\bar{M}$ point lies in the proximity or the possible overlap of the bulk and surface bands, which promotes the strong electron scattering between the surface and bulk, and smears the surface band around the $\bar{M}$ point.

To demonstrate the evolution of surface states in a wide x range, we plot in Fig. 4 the ARPES intensity along the $\bar{\Gamma}\bar{M}$ cut near the $\bar{\Gamma}$ point for various Sb concentrations, including pristine Bi ($x = 0.0$) and Sb ($x = 1.0$).[27] At the $\bar{\Gamma}$ point, we observe the spin-split Σ_1 and Σ_2 bands. Obviously, the spin-split bands gradually expand in energy and the Kramers point gradually shifts down for increasing values of x. Simultaneously, the separation of Fermi vectors (k_F) between the Σ_1 and Σ_2 bands becomes narrower, as clearly recognized for $x = 1.0$. Such a band evolution as a function of x is related to the variation of the SOC strength. To clarify this point quantitatively, we fit the peak position of EDCs (circles) by assuming a simple parabolic band dispersion with a Rashba splitting, as expressed by $E(k) = a(k \pm \Delta k)^2 - E_0$, where $2\Delta k$ is the momentum separation of spin-split bands and E_0 is the bottom of the energy band. The estimated $2\Delta k$ values are 0.11, 0.09, 0.08, and 0.05 Å^{-1} for $x = 0.0$, 0.023, 0.17, and 1.0, respectively, which suggests the monotonous reduction of SOC strength at the surface with Sb substitution. The gradual downward shift of the band bottom essentially tracks the trend of the reduced SOC in the band calculation of surface layers,[25] which is consistent with the reduced SOC that was also discussed in a previous ARPES study on Sb(111).[27] We think that this behavior is a direct manifestation of the reduction of bulk SOC, and therefore the bulk-band inversion at the L point—a prerequisite for the realization of the TI phase—would be explained well by the change in the strength of bulk SOC as a function of x.

The present result thus establishes that the topological phase transition is directly related to the appearance or absence of the Σ_1' band around the $\bar{M}$ point. A question therefore arises as to the energy location of the Σ_1' band in the non-TI phase. One possibility is that it is originally located above E_F in the low-x region and is pulled down below E_F with increasing values of x. The experimental fact that the Σ_1 band is located at higher binding energy at larger values of x [see Fig. 3(c)] may be compatible with this scenario, whereas the Σ_1' band is not clearly seen above E_F for $x = 0.023$ [see Fig. 2(g)], probably because of the thermal broadening and resultant smearing of the weak Σ_1' feature at high temperatures. Another possibility is that the appearance of the Σ_1' band is a consequence of the hybridization between the Σ_1 band and the trivial surface state below E_F, as indicated by the *ab initio* calculations.[21] In this case, the trivial surface state would suffer strong x dependence in its energy position and/or its spectral weight, since no indication of such a trivial surface state was found in $x = 0.023$. In either case, the appearance of the Σ_1' band could be closely related to the variation of the SOC strength, as revealed by the x dependence of the band dispersion around the $\bar{\Gamma}$ point.

In conclusion, we have performed a high-resolution ARPES study of $Bi_{1-x}Sb_x$ alloys as a function of Sb concentration (x = 0.0, 0.023, 0.17, and 1.0). By determining the FS and the band structure, we found that the topological phase transition is accompanied by the emergence of the Σ_1' band in the vicinity of E_F around the $\bar{M}$ point. The present ARPES result also provides evidence for the systematic reduction of the SOC parameter with Sb substitution, which may be a prerequisite for the band inversion responsible for the topological phase transition in $Bi_{1-x}Sb_x$.

This work was supported by grants from JST-CREST, JSPS, and MEXT of Japan. A.T. thanks JSPS for financial support.

[1] B. A. Bernevig, T. L. Hughes, and S.-C. Zhang, Science **314**, 1757 (2006).
[2] M. König, S. Wiedmann, C. Brüne, A. Roth, H. Buhmann, L. W. Molenkamp, X.-L. Qi, and S.-C. Zhang, Science **318**, 766 (2007).
[3] P. Cheng, C. Song, T. Zhang, Y. Zhang, Y. Wang, J.-F. Jia, J. Wang, Y. Wang, B.-F. Zhu, X. Chen, X. Ma, K. He, L. Wang, X. Dai, Z. Fang, X. Xie, X.-L. Qi, C.-X. Liu, S.-C. Zhang, and Q.-K. Xue, Phys. Rev. Lett. **105**, 076801 (2010).
[4] H. Peng, K. Lai, D. Kong, S. Meister, Y. Chen, X.-L. Qi, S.-C. Zhang, Z.-X. Shen, and Y. Cui, Nature Mater. **9**, 225 (2010).
[5] A. A. Taskin and Yoichi Ando, Phys. Rev. B **80**, 085303 (2009).
[6] D.-X. Qu, Y. S. Hor, J. Xiong, R. J. Cava, and N. P. Ong, Science **329**, 821 (2010).
[7] J. G. Analytis, R. D. McDonald, S. C. Riggs, J.-H. Chu, G. S. Boebinger, and I. R. Fisher, Nature Phys. **6**, 960 (2010).
[8] D. Hsieh, D. Qian, L. Wray, Y. Xia, Y. S. Hor, R. J. Cava, and M. Z. Hasan, Nature (London) **452**, 970 (2008).
[9] D. Hsieh, Y. Xia, L. Wray, D. Qian, A. Pal, J. H. Dil, J. Osterwalder, F. Meier, G. Bihlmayer, C. L. Kane, Y. S. Hor, R. J. Cava, and M. Z. Hasan, Science **323**, 919 (2009).
[10] A. Nishide, A. Taskin, Y. Takeichi, T. Okuda, A. Kakizaki, T. Hirahara, K. Nakatsuji, F. Komori, Y. Ando, and I. Matsuda, Phys. Rev. B **81**, 041309(R) (2010).
[11] T. Hirahara, Y. Sakamoto, Y. Saisyu, H. Miyazaki, S. Kimura, T. Okuda, I. Matsuda, S. Murakami, and S. Hasegawa, Phys. Rev. B **81**, 165422 (2010).
[12] M. Z. Hasan and C. L. Kane, Rev. Mod. Phys. **82**, 3045 (2010).
[13] Y. Xia, D. Qian, D. Hsieh, L. Wray, A. Pal, H. Lin, A. Bansil, D. Grauer, Y. S. Hor, R. J. Cava, and M. Z. Hasan, Nature Phys. **5**, 398 (2009).
[14] Y. L. Chen, J. G. Analytis, J.-H. Chu, Z. K. Liu, S.-K. Mo, X. L. Qi, H. J. Zhang, D. H. Lu, X. Dai, Z. Fang, S. C. Zhang, I. R. Fisher, Z. Hussain, and Z.-X. Shen, Science **325**, 178 (2009).
[15] T. Sato, K. Segawa, H. Guo, K. Sugawara, S. Souma, T. Takahashi, and Y. Ando, Phys. Rev. Lett. **105**, 136802 (2010).
[16] K. Kuroda, M. Ye, A. Kimura, S. V. Eremeev, E. E. Krasovskii, E. V. Chulkov, Y. Ueda, K. Miyamoto, T. Okuda, K. Shimada, H. Namatame, and M. Taniguchi, Phys. Rev. Lett. **105**, 146801 (2010).
[17] Y. L. Chen, Z. K. Liu, J. G. Analytis, J.-H. Chu, H. J. Zhang, B. H. Yan, S.-K. Mo, R. G. Moore, D. H. Lu, I. R. Fisher, S. C. Zhang, Z. Hussain, and Z.-X. Shen, Phys. Rev. Lett. **105**, 266401 (2010).
[18] P. Roushan, J. Seo, Colin V. Parker, Y. S. Hor, D. Hsieh, D. Qian, A. Richardella, M. Z. Hasan, R. J. Cava, and A. Yazdani, Nature (London) **460**, 1106 (2009).
[19] J. Seo, P. Roushan, H. Beidenkopf, Y. S. Hor, R. J. Cava, and A. Yazdani, Nature (London) **446**, 343 (2010).
[20] L. Fu and C. L. Kane, Phys. Rev. B **76**, 045302 (2007).
[21] H.-J. Zhang, C.-X. Liu, X.-L. Qi, X.-Y. Deng, X. Dai, S.-C. Zhang, and Z. Fang, Phys. Rev. B **80**, 085307 (2009).
[22] J. C. Y. Teo, L. Fu, and C. L. Kane, Phys. Rev. B **78**, 045426 (2008).
[23] S. Souma, A. Takayama, K. Sugawara, T. Sato, and T. Takahashi, Rev. Sci. Instrum. **78**, 123104 (2007).
[24] C. R. Ast and H. Höchst, Phys. Rev. Lett. **87**, 177602 (2001).
[25] Yu. M. Koroteev, G. Bihlmayer, J. E. Gayone, E. V. Chulkov, S. Blügel, P. M. Echenique, and Ph. Hofmann, Phys. Rev. Lett. **93**, 046403 (2004).
[26] L. Fu, C. L. Kane, and E. J. Mele, Phys. Rev. Lett. **98**, 106803 (2007).
[27] K. Sugawara, T. Sato, S. Souma, T. Takahashi, M. Arai, and T. Sasaki, Phys. Rev. Lett. **96**, 046411 (2006).